PREDICTION OF COLLOID RETENTION ON NONSILICA SURFACES USING REPRESENTATIVE DISCRETE HETEROGENEITY

by

Jacob Scott Trauscht

A thesis submitted to the faculty of
The University of Utah
in partial fulfillment of the requirements for the degree of

Master of Science

in

Geological Engineering

Department of Geology and Geophysics

The University of Utah

August 2015

The University of Utah Graduate School

STATEMENT OF THESIS APPROVAL

The thesis of **Jacob Scott Trauscht**

has been approved by the following supervisory committee members:

William P. Johnson	, Chair	**6/9/2015** Date Approved
John Bowman	, Member	**6/9/2015** Date Approved
David Grainger	, Member	**6/9/2015** Date Approved

and by **John Bartley** , Chair/Dean of

the Department/College/School of **Geology and Geophysics**

and by David B. Kieda, Dean of The Graduate School.

ABSTRACT

Despite several decades of research there currently exists no mechanistic theory to predict deposition in porous media in the presence of colloid-collector repulsion (unfavorable conditions). Recently, mechanistic models have been developed that incorporate nanoscale surface heterogeneity in colloid-collector interactions. Comparison of simulations to experimental data allows backing out a representative heterogeneity for the surface, which to date has been reported only for silica. Colloid deposition onto a variety of representative aquifer materials expected to be unfavorable under environmental conditions (amorphous silica, muscovite and albite) was observed for 0.25, 1.1 and 2.0 μm carboxylate-modified latex microspheres using an impinging jet system. Deposition efficiencies varied in response to changes in collector mineralogy, ionic strength, electrolyte valence and pH. Characteristics (size and spatial distribution) of surficial charge-heterogeneity on the collector were backed out from these experiments via comparison to particle trajectory simulations incorporating discrete nanoscale attractive domains (heterodomains). A bimodal distribution (1:4, ratio of large to small heterodomains) of 120nm and 60nm diameter heterodomains was found to predict attachment onto silica across the range of colloid sizes, solution chemistries and fluid velocities, whereas a uniform distribution of 120nm heterodomains was found to predict retention on muscovite. Varying the surface coverage of heterodomains allowed a characteristic coverage for each observed collector surface to be determined. This

developing catalog of surface characteristics will aid prediction of colloid transport and deposition under environmentally relevant conditions (aquifer material composition and groundwater chemistry). This study also highlighted the fact that heterogeneity on the collector surface alone is not enough to capture trends in deposition across the range of minerals and solution chemistries examined and more mechanisms of attachment need to be examined.

TABLE OF CONTENTS

LIST OF TABLES

LIST OF FIGURES

ACKNOWLEDGEMENTS

I am grateful for all the help and dedication from my advisor, Dr. Bill Johnson. In addition, Eddy Pazmino, for all of his help during all aspects of my research and the entire geology and geophysics staff for their help. I would also like to thank my Committee members, John Bowman and David Grangier, for their help and input during the creation of this manuscript. I am also grateful for the technical and facility support provided at the Center for High Performance Computing, the Rocks Mechanics Lab and the Electron Microprobe lab at the University of Utah. This research was supported by the U.S. National Science Foundation Hydrologic Sciences Programs (award 1215726). Any opinions, findings, and conclusions or recommendations expressed in this material are those of the authors and do not necessarily reflect the views of the National Science Foundation.

CHAPTER 1

BACKGROUND

The presence of contaminants in aquifers is an ever-growing problem facing the global population as groundwater is increasingly used for human consumption and agriculture. While traditionally groundwater has been considered clean relative to surface water, increased presence of pollutants from anthropogenic sources including agriculture, mining, oil and gas drilling and human waste means this assumption is no longer valid. The presence of contaminants in aquifers highlights the importance of understanding how contaminants are transported through, and filtered out of, groundwater. Dissolved contaminants are modeled at the continuum scale using an empirically derived coefficient (K_D) for equilibrium distribution of the contaminant between water and sediment. This equilibrium is achieved because of high diffusion rates and K_D is assigned for a particular contaminant-sediment system. In contrast there is no equilibrium between colloids and surfaces, and so the filtration is dependent on many more variables relative to K_D. Current theory can predict filtration of particles in engineered porous media systems well but fails to predict particle filtration under environmentally relevant conditions, such as those found in groundwater. Understanding particle filtration in natural porous media allows for prediction of particle transport, which has many practical implications including: calculation of set-back distances between a contaminant source and drinking water,

prediction of travel distances of contaminants associated with particles, design of low-energy filtration systems such as riverbank filtration, and targeted delivery of bacteria or engineered nanoparticles for remediation of dissolved contaminants (Zhang, 2003; Weiss et al., 2005).

Particle filtration in porous media does not occur primarily via straining in which a particle is arrested because it is larger than a pore throat. Instead, particle filtration is dominated by particle delivery to the surface of a grain where a particle must be on a fluid streamline within a flow field that intercepts a grain to be arrested on the grain surface (Rajagopalan and Tien, 1976). Particles in the size range of 50 nm to a 1000 nm, referred to as colloids, are of particular interest as diffusion is overcome by settling for larger colloids. These mechanisms result in enhanced filtration of larger and smaller colloids that is observed in experimental observations (Tong et al., 2006; Pazmino et al., 2011). Transport of colloids to a surface is quantified via the collector efficiency (η) and is defined as:

$$\eta_{fav} = \frac{\#colloids\ deliverd\ to\ surface}{\#colloids\ injected}$$

Traditional colloid filtration theory predicts collector efficiency well for systems in which a grain (herein called 'collector') and a colloid are oppositely charged where it is assumed all colloids delivered to a surface attach, conditions that are referred to as 'favorable.' However, systems in which colloids and collectors are both negatively charged, a condition found in the environment, colloid-collector repulsion exists and traditional colloid filtration theory predicts zero attachment (Elimelech and O'Melia, 1990).

The presence or absence of colloid-collector repulsion is primarily due to the presence of DLVO forces that describe the force between charged surfaces acting through a medium.

DLVO forces arise from a combination of close range van der Waals forces, which are generally attractive, and farther ranging electric double layer (EDL) forces that can be attractive or repulsive depending on the charge of the colloid and collector (Israelachvili, 2011). This charge is quantified via the ζ-potential that arises from the electrical potential difference between the medium and ions associated with the surface, which remain present at the surface in the presence of fluid shear. Under favorable conditions the ζ-potential of the colloid and collector are oppositely charged and result in attractive forces, creating colloid-collector attraction (Figure 1a). However, when a colloid and collector both have negative ζ-potentials, the forces due to the electric double layer are repulsive and overcome attractive van der Waals forces, creating colloid-collector repulsion (Figure 1b). Decreasing the ionic strength causes the EDL to extend further into solution, and also increases the magnitude of the ζ-potential of the colloid and collector, which results in an increase in the height of the force barrier (Figure 1b). Presence of colloid-collector repulsion due to these DLVO forces results in classic colloid filtration theory predicting zero attachment under unfavorable conditions.

Despite the presence of colloid-collector repulsion, experimental observations demonstrate that colloid filtration occurs under unfavorable conditions. Filtration under unfavorable conditions is also quantified via the collector efficiency (η), but it is not valid to assume all colloids that get to a surface will attach and the definition changes to recognize this:

$$\eta_{unf} = \frac{\#colloids\ attached\ to\ surface}{\#colloids\ injected}$$

Under unfavorable conditions only a fraction of the colloids that are delivered to the surface attach. This fraction can be represented by an experimentally determined factor

called the collision efficiency (α), which ranges from 0 to 1 (1 being favorable conditions) and is defined as (Elimelech, 1992):

$$\propto = \frac{\eta_{unf}}{\eta_{fav}}$$

One approach to predicting α employs semi-empirical equations that rely upon both empirically derived constants and system parameters (i.e., ionic strength, ζ-potential, Hamaker constant) (Elimelech, 1992; Bai and Tien, 1999; Chang et al., 2009). This approach predicts η_{unf} via the product of the calculated collision efficiency (α) and η_{fav}, which can be calculated using classic colloid filtration theory. While this approach works under the experimental conditions for which the equations were developed, it relies heavily upon empirically derived constants and does not attempt to explain the physics that allow colloid attachment in the presence of colloid-collector repulsion.

An alternative approach to the empirically derived collision efficiency attempts to understand the physics that allow colloid deposition onto a surface in the presence of an energy barrier. This theory hypothesizes that areas of nanoscale surface heterogeneity (i.e., surface roughness or charge) locally eliminate the barrier to attachment (Hoek et al., 2003; Duffador et al., 2007). More recently, a model that represents this nanoscale heterogeneity as charge heterogeneity (heterodomains) was developed that tracks a particle from introduction to the system until the colloid either attaches to a heterodomain or exits the system (Pazmino et al., 2014). This approach successfully modeled colloid filtration for a range of colloid sizes (0.25 – 2.0 μm), ionic strengths (6 and 20 mM) and fluid velocities (1.71 and 5.94 mm/s) but was limited to silica collector surfaces, a single pH and a 1:1 electrolyte (NaCl). While this model was impressive in its scope, aquifers are comprised of a variety of minerals, electrolyte types and pH ranges. The goal of this thesis is to

understand the effect of mineralogy, electrolyte type and pH on colloid filtration and determine if this model is able to successfully simulate filtration under these environmentally relevant conditions.

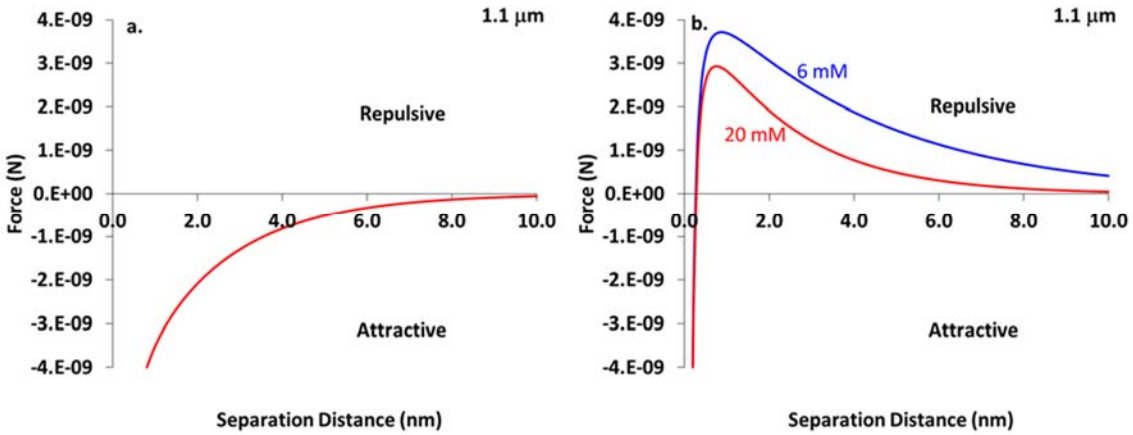

Figure 1 Calculated DLVO forces for favorable (a) and unfavorable (b) conditions as a function of separation distance for a 1.1 µm colloid in a 1:1 electrolyte solution. For the unfavorable condition two different ionic strengths are shown (orange solid line = 6 mM, red solid line = 20 mM).

CHAPTER 2

INTRODUCTION

Filtration of nano- and microparticles (herein referred to as colloids) in environmental granular media is the predominant process in practical environmental engineering applications such as design of low-energy water treatment systems, e.g., river bank filtration (Weiss et al., 2005), and targeted delivery of engineered nanoparticles for subsurface remediation (Zhang, 2003). A major challenge in the design of such systems is predicting the attachment of colloids to surfaces in the presence of colloid-surface repulsion that typically exists under environmental conditions, so-called unfavorable conditions for attachment. Prediction of attachment is performed via simulation of colloid trajectories based on force and torque balances in a 'collector' that represents porous medium as a spherical grain with a fluid envelope having a thickness that corresponds to the porosity of the media being considered (Yao et al., 1971; Rajagopalan and Tien, 1976), and a flow field reflecting the continuum of fluid velocities from zero at the grain surface to a maximum at the "divide" separating fields associated with adjacent collectors (Rajagopalan and Tien, 1976). The fraction of all simulated colloids entering the collector that reach the near-surface fluid domain (the fluid within approximately 200 nm of the grain surface) is quantified as the collector efficiency (η). The value of η is determined as a function of porosity, colloid size, fluid velocity, solution ionic strength (IS). Colloid

retention predicted from η matched observed retention in simplified systems such as spherical colloids in uniform porous media (i.e., cubic packing) under conditions lacking colloid-collector repulsion (favorable conditions, η_{fav})(Elimelech and O'Melia, 1990; Johnson and Tong, 2006).

To provide easily implemented mechanistically-based predictive capability under favorable conditions, the mechanistic simulations have been approximated by correlation equations (Rajagopalan and Tien, 1976; Tufenkji and Elimelech, 2004). Colloid-collector attraction or repulsion is due to the presence of the electric double layer and is defined by a mean field parameter the ζ-potential. Under favorable conditions no colloid-collector repulsion exists due to oppositely charged double layer potentials (opposite ζ-potential signs) and all colloids that reach the near surface will attach. The number of colloids removed solution via filtration is quantified by the collector efficiency (η), and is defined as:

$$\eta_{fav} = \frac{\#colloids\ delivered\ to\ surface}{\#colloids\ injected\ into\ system}$$

While the conventional force/torque balance approach predicts collector efficiency (η_{fav}) well for favorable conditions, this approach fails under unfavorable conditions. This is because conventionally predicted colloid-surface repulsion in mechanistic force/torque balances prevents colloid attachment under unfavorable conditions (Elimelech and O'Melia, 1990). Since unfavorable conditions are considered typical of environmental contexts, this result is a major challenge for colloid transport prediction in the environment. Current predictions of collection efficiency (η_{unf}) under unfavorable conditions rely upon an experimentally derived factor known as the collision efficiency (α)(Elimelech, 1992),

which represents the ratio of unfavorable (η_{unf}) and favorable (η_{fav}) collector efficiencies:

$$\alpha = \frac{\eta_{unf}}{\eta_{fav}} = \frac{\left[\frac{\#colloids\ attached}{\#colloids\ injected\ into\ system}\right]}{\left[\frac{\#colloids\ delivered\ to\ surface}{\#colloids\ injected\ into\ system}\right]} = \frac{\#colloids\ attached}{\#colloids\ delivered\ to\ surface}$$

A number of easily implemented semi-empirical (not mechanistic) expressions for prediction of α (Elimelech, 1992; Bai and Tien, 1999; Chang et al., 2009), have been developed the goal being to use the product of η_{fav} and α to predict colloid retention under unfavorable conditions (η_{unf}). These semi-empirical correlations for predicting α were developed in glass-bead or quartz-sand porous media. They have not, to the knowledge of the authors, been tested in porous media that contain other minerals, or outside the range of experimental parameters from which they were developed.

The failure of mechanistic force/torque balance to predict colloid attachment under unfavorable conditions arises from the fact that colloid-surface interaction used in these trajectory simulations are estimated using mean-field DLVO theory, where the surface potentials of the colloid and collector (approximated by zeta potentials) are assumed homogenous across the surfaces. The likely influence of nano- to microscale charge heterogeneity and roughness to locally reduce or eliminate colloid-collector repulsion has long been recognized (Elimelech and O'Melia, 1990; Song et al., 1994). However, only recently has discrete nano- to microscale heterogeneity been incorporated into DLVO theory for purposes of quantitative prediction of colloid retention under unfavorable conditions for a variety of colloid sizes, fluid velocities, and solution ionic strengths (Duffadar and Davis, 2008; Duffadar et al., 2009; Pazmino et al., 2014a). Currently there exist no easily implemented predictions based on these mechanistic simulations.

Prediction of colloid retention in granular media having macroscopic heterogeneity

(e.g., measurable favorable surfaces) can be successfully approximated using a simple linear combination of α values, where α is equal to 1 for favorable conditions and assumed to be zero for unfavorable conditions (Johnson et al., 1996; Loveland et al., 2003; Laumann et al., 2014) . However, this approach is not practicable in media where bulk favorable surfaces are absent, and heterogeneity responsible for attachment is micro- or sub-microscopic, because the linear approximation incorrectly predicts zero attachment in such media. However, the inferred microscale heterogeneity is not directly measurable via methods directly relevant to colloid-surface interaction, as evidenced by its insignificant influence on the measured zeta potential (ζ) (Elimelech et al., 2000b)).

Recent successful mechanistic predictions of colloid attachment under unfavorable conditions in macroscopically uniform granular media incorporate discrete nano- to micro-scale "heterodomains" in the estimation of colloid-surface interactions (Hoek et al., 2003; Duffadar and Davis, 2007; Duffadar et al., 2009; Ma et al., 2011). The heterodomains, zones of attractive electrical potential on otherwise bulk repulsive surfaces, may locally reduce or eliminate the repulsive electrostatic barrier. Whether the overall colloid-surface interaction is net attractive or net repulsive depends on the fraction of the zone of interaction (ZOI) that is occupied by heterodomain(s) (Duffadar and Davis, 2007; Duffadar et al., 2009; Bendersky and Davis, 2011; Pazmino et al., 2014a). The radius of the ZOI is approximated as:

$$R_{ZOI} \approx 2\sqrt{\kappa^{-1}a_p}$$

where κ^{-1} is the Debye length and a_p is the particle radius. Since the ZOI is directly related to colloid size and inversely related to IS through the Debye length, colloid-surface interactions depend not only on heterodomain size, but also on colloid size and solution IS.

When this discrete heterogeneity approach is applied to collector geometries that include a grain-to-grain contact, the various observed modes of colloid retention under unfavorable conditions (e.g., wedging of colloids < 2 μm in diameter in grain-to-grain contacts) emerge from the force/torque balance (Ma et al., 2011).

More recently, Pazmino et al. (2014a) determined a representative discrete heterogeneity for silica surfaces by comparison of simulations to observed attachment of carboxylate-modified polystyrene latex microspheres (CML) under unfavorable conditions for CML sizes ranging 0.25 to 2.0 μm (diameter), fluid velocity ranging from 1.71×10^{-3} m/s to 5.94×10^{-3} m/s, and IS ranging from 6mM to 20mM for NaCl as the electrolyte at pH 6.7. This array of experiments was well described with a representative discrete heterogeneity having Pareto size-distributed heterodomains (approximated with 60 nm and 120 nm radii) at a total surface coverage of 0.04%. This representative discrete heterogeneity approach not only quantitatively predicted CML retention on silica, but also qualitatively predicted CML detachment from silica in response to perturbations of IS or flow (Pazmino et al., 2014b). The discrete heterogeneity approach is unique in that, using the same set of mechanistic parameters, it can predict attachment to surfaces, and qualitatively predict detachment via perturbations.

The success of the discrete heterogeneity approach for CML deposition on silica holds promise for expanding this construct to other unfavorable surfaces and solution chemistries that exist in natural porous media. For example, column-and-pore scale experiments show strong influences of pH (Abbott et al., 1983; Jewett et al., 1995), surface ζ-potential (Elimelech et al., 2000a; Kirby and Hasselbrink, 2004; Liu et al., 2014), and electrolyte valence (Liu et al., 1995; Chen and Walker, 2007). The objective of this research is to

extend the discrete heterogeneity approach to additional environmentally relevant collector materials and solution chemistries. It is an open question whether the representative discrete heterogeneity that successfully represented CML interaction with silica at pH 6.7 with NaCl electrolyte will also succeed at higher pH and in the presence of other electrolytes. Furthermore, it is not clear whether CML interaction with mineral surfaces other than silica can be modeled using the discrete heterogeneity approach. To explore these questions we performed experiments on a variety of unfavorable mineral surfaces (silica, muscovite, sodium-feldspar), at multiple solution pH values (6.7-8.0), and multiple solution electrolyte types (NaCl, $CaSO_4$, $CaCO_3$-dominated synthetic groundwater) for a range of CML sizes (0.25 μm-2.0 μm), fluid velocities (1.71×10^{-3} m/s to 5.94×10^{-3} m/s). Discrete heterogeneity simulations were conducted to determine whether this approach was able to capture the experimental results, and to determine whether the representative discrete heterogeneity characteristics (heterodomain size, distribution and surface coverage) differed for different minerals, pH conditions, and electrolytes. The comparison highlights strengths and weakness of the representative discrete heterogeneity approach to modeling observed colloid attachment.

CHAPTER 3

METHODS

3.1 Microspheres

Carboxylate-modified polystyrene fluorescent (λ_{ex} 505, λ_{ex} 515 nm) microspheres (Molecular Probes, Inc., Eugene, OR) of three sizes (0.25, 1.1 and 2.0 μm in diameter) were used in the experiments. Colloid suspensions were prepared from stock in relevant solution to the required concentrations of $5x10^6$, $3.5x10^6$, and $2x10^6$ microspheres per mL for the 0.25, 1.1 and 2.0 μm colloids, respectively. Injection concentration was determined via vacuum filtration of colloid solution with a 0.1 μm filter (MILLIPORE, Ireland) followed by averaging counts of 25 random areas using wide-field fluorescence for colloid illumination (see below for details on illumination). The ionic strength (IS) was adjusted using either NaCl, $CaSO_4$ or artificial groundwater (AGW) matching water of the Snake River aquifer (see Appendix) (Ferris et al., 2004). All solutions were buffered with 2.2 mM MOPS with pH set to 6.7 and 8.0 using NaOH (0.5M). Colloid ζ-potentials were calculated from electrophoretic mobility (EPM) via the Smoluchowski equation (Ohshima, 1995). EPM was measured in experimental solutions using a ζ-potential analyzer (Mobiuζ, Wyatt Technology Corp., Santa Barbara, CA). ζ-potential values for all colloid sizes and conditions are reported in the Appendix.

3.2 Collector Preparation

3.2.1 Surface properties

Soda-lime glass microscope slides (Fisher Scientific, Inc.), synthetic muscovite sheets (Electron Microscopy Sciences, Hatfield, PA), and thin sections of albite and labradorite (prepared by University of Utah rock preparation laboratory) were each used as impinging surfaces for retention experiments. Previous to every experiment, slides were cleaned via the SC-1 procedure (Kern, 1970). Silica slide ζ-potential in NaCl solutions were obtained from literature when available and are reported in the Appendix (Kirby and Hasselbrink, 2004). Silica slide ζ-potential in AGW and $CaSO_4$ solutions were obtained via EPM measurements as described above for colloid suspensions. A combined Hamaker constant for the silica-water-polystyrene system was taken from the literature ($A_{132} = 3.84 \times 10^{-21}$ J) (Israelachvili, 2011). Silica-slide suspensions were developed by crushing 0.3 g samples using mortar and pestal with suspension in 15 mL of the relevant solution (varied as described above) for 30 minutes to allow larger particles to settle. Freshly cleaved synthetic muscovite sheets showed no significant difference in η with versus without SC-1 cleaning. Muscovite ζ-potentials were averaged from several publications and are reported in the Appendix (Scales et al., 1990; Adamczyk et al., 2010). A combined Hamaker constant (A_{132}) for muscovite (phase 1) interacting with polystyrene (phase 2) across water (phase 3) was not available in the literature so a value was determined using the approximation below, as subscripted for the three phases (Israelachvili, 2011):

$$A_{132} \approx (\sqrt{A_{11}} - \sqrt{A_{22}})(\sqrt{A_{22}} - \sqrt{A_{33}})$$

where A_{ii} is the Hamaker constant of polystyrene, muscovite, silica, or water in vacuum. The Hamaker constant of muscovite in vacuum was averaged from three sources and is

$8.9x10^{-20}$ J (Ackler et al., 1996; Bergström, 1997; Israelachvili, 2011). Hamaker constants for polystyrene and water in vacuum were taken from the literature and are $6.5x10^{-20}$ J and $3.7x10^{-20}$ J, respectively (Israelachvili, 2011).

$$A_{132} \approx \left(\sqrt{8.9x10^{-20}} - \sqrt{6.5x10^{-20}}\right)\left(\sqrt{6.5x10^{-20}} - \sqrt{3.7x10^{-20}}\right) = 2.72x10^{-21}$$

Thin sections of albite (University of Utah rock preparation laboratory) were mounted on silica slides for use in the impinging jet experiments. SC-1 cleaning was used on thin section samples but resulted in destruction of the thin section after 4 uses. Albite thin sections were initially cleaned using a common thin section cleaning method of ethanol/acetone/water baths but this resulted in increased collector efficiencies after subsequent cleanings. A modified cleaning procedure was developed for albite consisting of sonication for 1 minute in 190 proof ethanol followed by a acetone/ethanol/millQ water rinse, followed by 1 hour bath in 30% hydrogen peroxide and a final rinse with milliQ water. The modified cleaning procedure resulted in reproducible experimentally observed colloid deposition in impinging jet experiments. Albite composition was determined using microprobe analysis via wavelength dispersive X-ray spectroscopy (University of Utah microprobe laboratory). The albite was determined to be 75% albite, 24% anorthite and 1% orthoclase.

ζ-potential for albite was determined via EPM as described above for colloid suspensions. Albite was pulverized using a mortar and pestal and added to relevant solution for 30 minutes to allow settling of larger particles. An aliquot (3 mL) was removed from supernatant and filtered (5.0 μm) (MILLIPORE, Ireland). EPM was measured in the filtrate. A Hamaker constant for albite in a vacuum was not available in existing literature; however, one was calculated on the basis of Lifshitz Theory (Israelachvili, 2011):

$$A_{ii} \approx \frac{3}{4} kT \left(\frac{\varepsilon_1 - \varepsilon_3}{\varepsilon_1 + \varepsilon_3}\right)^2 + \frac{3hv_e}{16\sqrt{2}} \frac{(n_1^2 - n_3^2)^2}{(n_1^2 + n_3^2)^{3/2}}$$

where k is the Boltzmann constant, T is temperature in kelvins, ε_1 is the dielectric constant of albite, ε_3 is the dielectric constant of the medium ($\varepsilon_3 = 1$ for a vacuum), h is Planck's constant, v_e is the mean electronic UV adsorption frequency for albite, n_1 is the refractive index of albite, n_3 is the refractive index of the solution (n_3=1 for vacuum).

The electronic adsorption frequency (v_e) was estimated to be $3x10^{15}$ since no value for albite could be found. However, other silicate minerals have similar values (Israelachvili, 2011).

The dielectric constant of albite was averaged from two sources (ε_1=6.5 +/- 0.5) (Rosenholtz, 1936; Olhoeft, 1989).

The refractive index of albite was averaged from the three principal crystal faces using the higher end of the ranges to reflect the presence of anorthite (n_1=1.535+/-0.004)(Deer et al., 2001).

$$A_{11} \approx \frac{3}{4}\left(1.38x10^{-23} \frac{m^2 kg}{s^2 K}\right)(298.15\ K)\left(\frac{6.5-1}{6.5+1}\right)^2$$

$$+ \frac{3\left(6.626x10^{-34} \frac{m^2 kg}{s}\right)(3x10^{15} s^{-1})}{16\sqrt{2}} \frac{(1.535^2 - 1^2)^2}{(1.535^2 + 1^2)^{\frac{3}{2}}} = 8.05x10^{-20}\ J$$

The combined Hamaker constant (A_{132}) for albite (1) interacting with polystyrene (2) across water (3) was determined using the same approximation used above for muscovite:

$$A_{132} \approx \left(\sqrt{8.05x10^{-20}} - \sqrt{6.5x10^{-20}}\right)\left(\sqrt{6.5x10^{-20}} - \sqrt{3.7x10^{-20}}\right) J$$

$$= 1.80x10^{-21}\ J$$

3.3 Impinging Jet Experiments

A custom-made, stainless-steel radial stagnation-point flow cell was used to observe colloid retention. Observations were made using an epifluorescence microscope with digital image capture, involving different illumination techniques for different impinging surfaces as described further below. The jet (cell inlet) was 0.50 mm in radius, and the impinging surface was located 1.22 mm perpendicular to the jet axis. To ensure an even radial distribution of the flow across the cell, four outlets were evenly spaced in a circular array at a radial distance 1 cm from the jet center. Experimental conditions were defined as low and high IS (6 and 20mM) and low and high average jet velocities (1.71×10^{-3} and 5.94×10^{-3} ms^{-1}). Colloid retention experiments were conducted by injecting colloidal suspensions (using a motorized syringe pump, Harvard Apparatus, Holliston, MA) into the flow cell after 30 min of equilibration with colloid-free solution. The duration of the experiments ranged from 1 to 14 h. A minimum of 20 colloid attachments on the observation area was considered representative.

Experiments examining deposition on glass used total internal reflection microscopy (Eclipse TE2000-S inverted microscope) (Nikon, Japan). A Melles Griot IMA 101 argon laser (Melles Griot Laser Group, Carlsbad, CA) was utilized to illuminate colloids. Experiments examining deposition on muscovite and albite utilized wide-field fluorescence with a band-pass-filter for excitation (478-493 nm) and a (405/488/543 nm) dichroic filter for emission (Chroma Technology Corp, Bellows Falls, VT) to illuminate colloids. Retention was quantified with images acquired every 15 s via a CoolSNAP HQ CCD camera (Photometrics, Tucson, AZ); a detailed description of the optical setup is provided in a previous publication (Johnson and Tong, 2006). During experiments a linear

slope of deposition versus time was observed, indicating that neither blocking nor ripening occurred during the experiments. An typical deposition history is shown in the Appendix.

3.4 Calculation of Collector Efficiency (η)

The colloid deposition rate across the area of observation (A_{obs}) was used to calculate the collector efficiency (η) via the following equation:

$$\eta = \frac{\left(\frac{\#attached}{time}\right)_{A_{OBS}}}{\left(\frac{\#injected}{time}\right)_{A_{JET}}} = \frac{\frac{\#attached}{time}}{C_o Q}$$

where C_O is the injected concentration of colloids and Q is the flow rate of the fluid that enters the cell (across the area of the jet, A_{jet}). The product C_OQ is equal to the number of particles injected per unit time across the area of the jet (A_{jet}). In simulations, colloid injection was performed across a smaller radius (R_{lim}) than R_{jet} for computational efficiency, since beyond this limiting radius (distance from the impinging jet axis) particles had zero chance of reaching the near surface fluid domain (e.g., Yang et al., 1998). An appropriate R_{lim} results in equivalent η despite increases in R_{lim} up to a limiting size where the number of colloids deposited becomes too small for accurate quantification (e.g., Pazmino, 2014a). The radius of the area of observation (A_{obs}) in simulations was chosen to enclose the same area as the experiment-based A_{obs} (450 × 336 μm^2), and served as the exit radius in the simulations. To ensure that the simulations were consistent with the lack of experimentally observed blocking (constant deposition rate), the number of colloids occupying discrete areas of positive charge (heterodomains) was confirmed to be less than 10% of total heterodomains.

3.5 Particle Trajectory Model Parameters

A Lagrangian particle trajectory model incorporating discrete heterogeneity to allow colloid attachment under unfavorable conditions (Pazmino, 2014a) was used to account for the various forces acting on the colloid, including fluid drag, hydrodynamic retardation, gravity, diffusion, colloid-surface interaction forces, and virtual mass. The electric double layer (EDL) force was calculated using an expression developed by Lin and Wiesner (2012), which is applicable to the ranges of IS and colloid size examined in this study (Lin and Wiesner, 2012). The retarded Van der Waals force for a plate-sphere system was calculated using an expression developed by Gregory (1981) employing the combined Hamaker constant (A_{132})(Gregory, 1981). A more detailed description of the force and torque balances, including fluid drag, hydrodynamic retardation, gravity, diffusion, steric forces and virtual mass are described in previous publications (Johnson and Tong, 2006; Ma et al., 2011; Pazmino et al., 2014a).

Parameters particular to experiments (Debye length (κ^{-1}), colloid size, ζ-potential) were used in calculation of the EDL force and the model was modified to allow a variety of electrolytes. This modification allows the Debye length to be calculated for a system containing a variety of electrolytes given ion concentration and valence of each ion. For calculation of the electric double layer forces in multivalent systems a mole weighted average was used for the valence ($z=1.2$ for AGW).

A previously published correlation equation for unfavorable conditions (Elimelech 1992) accounting for colloid/collector ζ-potentials, Debye length (κ^{-1}) and colloid size was also used to compare model performance. Although this correlation equation was developed using column tests, a comparison of the normal and tangential velocities

between the jet and column demonstrate the comparison is valid for the fluid velocities used in these experiments.

CHAPTER 4

RESULTS

4.1 Experimentally Observed η for Different Mineral and Solution Conditions

Experimentally observed collector efficiencies (η) determined from impinging jet experiments (shown as symbols in Figure 2) typically showed minima corresponding to the ca. 1-μm size range. We focus on collector efficiency (η) because the observed minimum value corresponding to the *ca.* 1-μm colloid size highlights critical information regarding the nature of heterogeneity on the surfaces, as discussed below. The minimum η corresponding to the *ca.* 1-μm colloid size was consistently observed across the range of ionic strengths (6 to 20 mM), range of pH (6.7 to 8), and range of fluid velocities (1.71 versus 5.94 mm/sec) (Figure 1). Minimum values of η for *ca.* 1-μm colloids under favorable conditions have been previously well demonstrated in porous media transport experiments (e.g., Tong et al., 2006; Pazmino et al., 2011).

For a given condition of IS, pH, and fluid velocity, silica yielded lower experimental η values (symbols) relative to muscovite and albite (Figure 1). For example, for the IS=6 mM, pH =6.7, v = 5.94 mm/sec condition (Figure 1b), silica yielded the lowest observed η values (red triangles), whereas mica (blue diamonds) yielded η values that reflected nearly

favorable conditions. The same was true for the same condition with IS elevated to 20 mM (Figure 1a), and also true (but reduced contrast) for the same conditions with reduced velocity to 1.71 mm/s (Figures 1c-d). Where examined at pH 6.7 (IS = 6 mM, v = 1.71 mm/s), albite produced results similar to muscovite (Figure 1d). The lack of significant variation of results for muscovite with varied IS and velocity at the pH 6.7 condition (Figure 1a-d) reflects the relatively favorable nature of this surface under this pH condition (Figure 2).

Muscovite and albite yielded η_{unf} results significantly lower than η_{fav} under elevated pH (Figure 2 e-f). Muscovite and albite yielded similar η values under conditions where they were both examined, except for elevated pH (8.0) and low IS (6 mM) (v = 1.71 mm/s), where muscovite yielded η values similar to silica (Figure 2f). This indicates a greater sensitivity of muscovite relative to albite to the pH increase. This greater sensitivity to pH increase from 6.7 to 8 observed for muscovite (at IS = 6 mM) (compare Figures 2 d and f), seems to reflect the higher isoelectric point of muscovite (pH 3.5) compared with silica and albite (pH 2.3 and 2.0, respectively) (Kosmulski, 2011).

4.2 Simulated η for Different Mineral and Solution Conditions

4.2.1 Semi-Empirical Correlations

The experimentally observed variation of η with colloid size, IS, pH and fluid velocity are potentially explained via force/torque balance simulations with the caveat that mean-field calculated colloid-surface interactions yield zero attachment. As a result, the only existing easily implemented method to predict η_{unf} is to employ existing semi-empirical expressions to predict α, and multiply α by the mechanistically predicted η_{fav} to obtain η_{unf}.

For the experimental conditions examined here, the best-performing semi-empirical expression for α was that of Elimelech (1992), as shown in Pazmino et al. (2015). The resulting predictions using the value of α estimated from Elimelech (1992) are shown as lines in Figure 2, which shows that trend as a function of colloid size (the characteristic minimum η_{unf} value corresponding to the ca. 1 μm colloid) is well captured by the semi-empirical prediction of Elimelech (1992). The expression has variable success in predicting CML attachment onto silica, with close match to observed η_{unf} under the pH 6.7 and 5.94 mm/s condition (both IS) (Figure 2 a and b), but poor match to observed η_{unf} under the pH 6.7 and 1.71 mm/s condition (both IS) (Figure 2 c and d). The predictions by the semi-empirical equation (Elimelech, 1992) show large under-prediction of observed values under all conditions examined for muscovite and (where examined) albite (Figure 2). The semi-empirical prediction was developed from experiments examining CML retention on silica (Elimelech, 1992) and, while it performs well for silica under particular conditions, it performs poorly for CML retention on muscovite and albite under all conditions examined here.

4.2.2 Discrete Heterogeneity Simulations

The poor performance of the semi-empirical correlation, combined with the fact that they are based on mean-field colloid-surface interactions, suggests the need to account for different surface characteristics of different mineral surfaces in prediction of η_{unf}. The discrete heterogeneity approach provides a means to build this specificity into CML-mineral interactions. Pazmino et al. (2014a) showed that retention of CML colloids on silica surfaces in impinging jet experiments was well described by colloid force/torque

balance simulations when a representative heterogeneity was used for silica that corresponded to a Pareto size distribution of heterodomains, as approximated using a 1:4 number ratio of 120 nm to 60 nm (radius) heterodomains at a surface coverage of 0.06%. This representative discrete heterogeneity simulated well the observed attachment of CML onto silica across the variety of IS and fluid velocities examined, but also simulated qualitatively the observed detachment in response to IS reduction and fluid velocity increase (Pazmino et al., 2014b).

Applying the approximate Pareto distribution to the larger range of conditions and surfaces examined here (Figure 3) shows that predictions generally match the observed values under the lower pH condition (6.7) (Figure 3 a-d), where different surface coverages by heterodomains were used for the three different minerals (0.06% for silica, 2.2% for muscovite, and 1.0% for albite). CML retention on silica at pH 8 was described using a surface coverage by heterodomains of 0.005%, an order of magnitude lower relative to that at pH 6.7 (Figure 3 e-f, red triangles and red lines). The reduction in heterodomain surface coverage may reflect an increased negative charge on the microsphere and silica surfaces as pH rises farther above the isoelectric point of silica (pH_{zpc} = 2.8). For CML retention on muscovite at pH 8, simulations with 0.01% surface coverage by heterodomains were able to marginally match the observed retention. However, the model poorly matched the experimentally observed trend in η as a function of colloid size (Figure 3 e-f); specifically, under predicting the retention of the 2 μm CML. For CML retention on albite at pH 8, a surface coverage by heterodomains of 0.07% described retention well for 0.25 and 1.1 μm colloids, but under-predicted (or over predicted) attachment of 2.0 μm colloids for the 20 mM (or 6 mM) IS condition (Figure 3 d - f).

An apparent shortcoming of the discrete heterogeneity simulations is the occasional over-complication of the trend in η as a function of colloid size, as described above. Specifically, under some conditions the simulated trends lack the characteristic minimum in η corresponding to the *ca.* 1 μm CML size (Figure 3), whereas the minimum is evident in nearly all experimental trends. Notably at high surface coverage by heterdomains, the simulated trends capture the experimental trends, and both show a minimum η corresponding to approximately 1.0 μm. Under conditions of high surface coverage by heterodomains (nearly favorable) the likelihood of approaching a heterodomain is high, and the likelihood of simulated retention is therefore dominated by colloid delivery to the near surface, as occurs for favorable conditions. At lower surface coverage by heterodomains, simulated trends in η as a function of colloid size may contrast against those simulated for higher surface coverages (compare Figures 3e and 3f). This contrast is explained by the fact that, as heterodomain surface coverage decreases, the probability of finding heterodomains of sufficient size to yield net attraction is decreased. The resulting trends in simulated η may not show minima corresponding to the 1.1 μm colloid size (Figure 3e). This results from a preponderance of small, relative to large, heterodomains (Pareto size distribution), the former serving as attachment sites for 1.1 μm colloids only under elevated IS. Specifically, at 6 mM IS, the larger colloids (1.1 and 2.0 μm) cannot attach to 60 nm heterodomains, restricting their attachment to 120 nm heterdomains only, resulting in similar attachment of these two colloid sizes under that condition (Figure 3 f). In contrast, at 20 mM IS, 1.1 μm colloids can attach to both 60 nm and 120 nm heterodomains while 2.0 μm colloids can only attach to 120 nm heterodomains, resulting in greater attachment of 1.1 relative to 2.0 μm colloids (Figure 3 e). Whereas Pareto size-

distributed heterodomains were previously inferred for silica surfaces (Pazmino et al., 2014a), such a distribution appears to over complicate the simulated trend of η as a function of colloid size for muscovite and albite at pH 8.0 (Figure 3 e and f).

The suboptimal match of simulations for muscovite and albite using representative discrete heterogeneity developed for silica highlights the possibility that the heterodomain size distribution differs for different minerals, and of course, these differences might be expected on the basis of different mineral structures for silica (amorphous) versus muscovite (phyllosilicate) versus albite (tectosilicate). Additionally, the different cation contents and substitutions expected among these minerals may play a role, their chemical formulas being SiO_2, $KAl_2(AlSi_3O_{10})(F,OH)_2$, and $Na_{0.75}Ca_{0.24}K_{0.01}AlSi_3O_8$ for silica, muscovite and albite, respectively. Notably, employing a uniform distribution of heterodomains (120 nm radius) for muscovite significantly improved the predicted trend of η as a function of colloid size, assuming a heterodomain surface coverage of 2.2% at pH 6.7 (Figure 4, a-d). However, the very significant influence of IS at pH 8 for CML-muscovite interactions was not captured by a single heterodomain surface coverage and requires an increase in heterodomain surface coverage to produce the range of attachment observed between 20 and 6 mM IS (Figure 4 e and f). Employing a uniform distribution of heterodomains (120 nm radius) for albite improves the predicted trend of η as a function of colloid size for the 20 mM, pH 8.0 condition assuming a heterodomain surface coverage of 0.07% (Figure 4e). At the 6 mM, pH 8.0 condition a uniform distribution of heterodomains does not improve the predicted trend in η as a function of colloid size for albite (Figure 4 f).

4.3 Observed and Simulated η on Silica for Different Electrolytes

Because natural groundwaters are not typically dominated by NaCl we examined the influence of divalent cations via use of $CaSO_4$ and AGW electrolytes, the latter dominated by calcium and bicarbonate. Divalent cations such as Ca^{2+} may act as cation bridges between like-charged negative moieties (Maier and Pepper, 2009), and have a factor of four greater influence on IS relative to 1:1 electrolytes. Both of these effects are expected to increase colloid retention. Experimentally determined η for CML deposition on silica in $CaSO_4$ and AGW solutions (Figure 5a) show that CML retention on silica was similar among the three electrolytes, with a maximum of one order of magnitude difference corresponding to the 2 μm CML. The primary observation is that the influence of cation bridging and elevated IS (from divalent electrolytes) did not greatly affect η under the relatively modest IS range examined here. Predicted η from the semi-empirical expressions (Elimelech, 1992) showed a poor match to experimental observations (Figure 5a), strongly over predicting the influence of IS on η for different electrolytes. Notably, predicted η from the representative discrete heterogeneity developed for CML deposition on silica in NaCl electrolyte (0.06% coverage by heterodomains) showed a much better match to experimentally observed CML deposition in $CaSO_4$ and AGW electrolytes (relative to semi-empirical prediction) (Figure 5b). The discrete heterogeneity predictions for $CaSO_4$ electrolyte reflected the experimentally observed η maximum corresponding to the 1 μm CML size; however, they did not reflect, for AGW electrolyte, the experimentally observed trend of increased η with increased CML size (Figure 5b). The discrete heterogeneity approach accurately predicted CML deposition on silica under multiple electrolytes using the a single discrete heterogeneity representation. This is a promising

outcome that reflects the model's dependence on ZOI and heterodomain size in addition to surface potential. Notably, large differences were observed in measured ζ-potentials for surfaces in NaCl versus divalent electrolyte solutions (see Appendix), leading to much higher sensitivity to electrolyte type for the semi-empirical correlation relative to the discrete heterogeneity predictions.

4.4 Observed and Simulated Detachment in Response to Perturbations

CML detachment in response to perturbations in flow (25x increase following deposition at 5.94 mm/s) and IS (reduction to 1 mM following deposition at 20 mM) was examined in experiments (Figure 6). The smallest CML (0.25 μm) showed insignificant detachment in response to both IS and velocity perturbations for all mineral surfaces examined, except for 20% detachment from silica in response to the IS perturbation at pH 8 (Figure 6). The larger colloids (1.1 and 2.0 μm) showed significant detachment (up to 60%) in response to flow perturbations at both pH values (Figure 6 a and b), and variable detachment in response to IS reduction (Figure 6 c and d). Detachment of larger colloids (1.1 and 2.0 μm) via flow perturbation was least for muscovite, and greatest for silica and albite (depending on CML size) at pH 6.7 (Figure 6a). In contrast, at pH 8, detachment of larger colloids (1.1 and 2.0 μm) via flow perturbations was significant for all mineral surfaces. Detachment for larger colloid sizes (1.1 and 2.0 μm) at pH 8.0 was similar among all three surfaces but somewhat greater for muscovite. This observation is consistent with the expected increasingly unfavorable colloid and mineral surfaces under pH conditions that are increasingly above the mineral isoelectric points (increasingly dominated by negative zeta potential). With respect to CML detachment via flow perturbation,

muscovite showed the greatest sensitivity to pH (Figure 6 a versus b), an effect that was also experimentally observed for CML attachment, and which reflects the higher isoelectric point of muscovite (3.5) vs silica (2.3) and albite (2.0) (Kosmulski, 2011). CML residence times for colloids that detached in response to velocity perturbations were significantly lower than colloids that remained for silica and muscovite, but no significant variation in residence times was observed for albite.

CML detachment in response to IS reduction to 1 mM was insignificant for muscovite and albite (Figure 6 c and d). CML detachment in response to IS reduction was significant for silica, with opposing trends in % detached as a function of CML size for pH 6.7 (direct relationship) versus pH 8.0 (inverse relationship) (Figure 6 c and d). The cause of the opposing trends is not known. Overall the detachment of CML from the three mineral surfaces was much greater for the 25x flow increase than for the IS reduction to 1 mM. Since the IS reduction is expected to eliminate secondary minima, the experimentally observed result also supports our underlying assumption that colloids were immobilized in primary minima.

Simulations of perturbations in fluid velocity and IS were performed using the results from simulated attachment (without changing parameters) to determine whether predicted detachment as a function of colloid size would qualitatively reflect experimental observations (Figure 6). Qualitative agreement with experiments was reported previously for silica in discrete heterogeneity simulations (Pazmino et al., 2014b). To the knowledge of the authors this (along with Pazmino et al., 2014b) is the first mechanistic model that predicts both attachment and detachment in response to perturbations in fluid velocity and solution IS using a single set of parameters. Simulations predicted detachment in response

to fluid velocity perturbations (Figure 6 a and b) and IS reduction (Figure 6 c and d), and in some cases there was qualitative correspondence to the experimentally observed trends (Figure 6b), and in others there was not (Figure 6d). In nearly all cases, the simulations over-predicted the observed detachment.

Two distinct driving mechanisms for detachment were examined: 1) release in response to increased fluid drag; and 2) release in response to decreased net attraction or even transition to net repulsion. In simulations, the likelihood of detachment in the simulations depends on: 1) colloid-surface separation distance upon attachment and colloid size (greater fluid velocities at greater distances from surface); 2) the fraction of ZOI occupied by heterodomains upon attachment (larger colloids have larger ZOI, and a given colloid's ZOI increases with increasing IS). Whereas the fluid drag force increased with colloid size, the strength of net attraction also increased with colloid size. This suggests that a cross-over occurred between driving fluid drag and resisting colloid-surface attraction such that predicted detachment in response to velocity perturbation was greatest for the 1-μm colloids, a trend that was reflected in some of the experimental trends (Figure 6b). Likewise, the potential for change from net attraction to net repulsion during IS reduction also depends on colloid size (to which are scaled colloid-surface interactions and ZOI). Both the simulations and experiments predict increased detachment with increased colloid size in response to IS reduction (Figure 6c). Furthermore, both simulations and experiments predict lesser detachment from muscovite relative to silica (Figure 6c); however, in contrast to simulations, the experimental data showed zero detachment from muscovite. The simulations did not predict the decreased detachment (in response to IS

reduction) with increased colloid size observed at pH 8, and that experimental trend is unexplained.

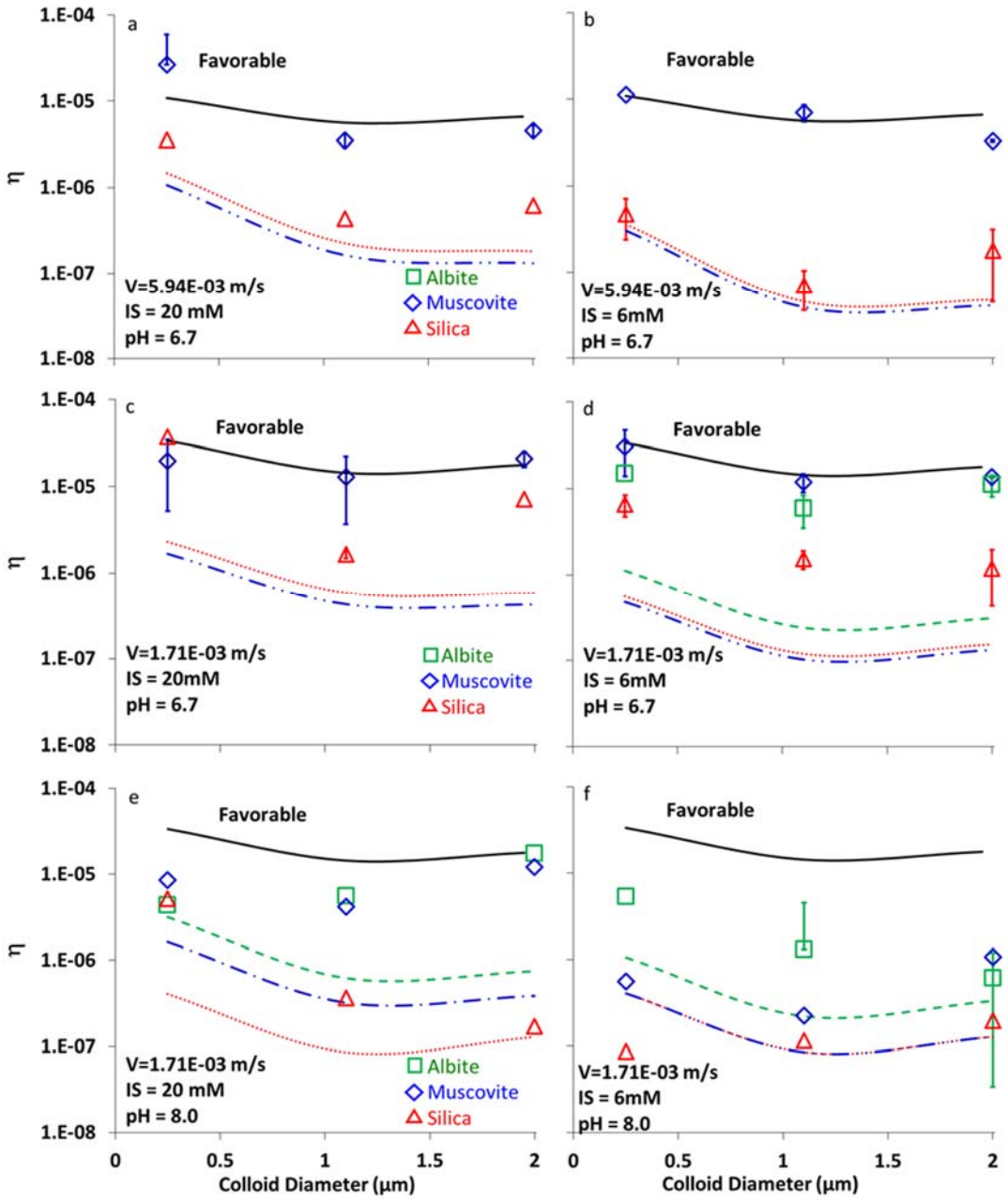

Figure 2 Experimentally observed collector efficiencies (η) as a function of colloid size for soda-lime glass (red triangles), muscovite (blue diamonds) and albite (green squares) at multiple ionic strengths (6mM, 20mM), pH values (6.7 and 8.0) and fluid velocities (1.71E-03, 5.94E-03 m/s). Lines are mechanistic force/torque balance simulation. Black solid lines represent favorable condition impinging jet simulations (mass transfer independent of mineral surface), with conversion to η. Colored textured lines represent unfavorable condition predictions (blue dash-dot=muscovite, red dots=glass, green dash=albite). Unfavorable condition predictions were performed using Elimelech (1992) to obtain α, which was multiplied by simulated by η_{fav} values.

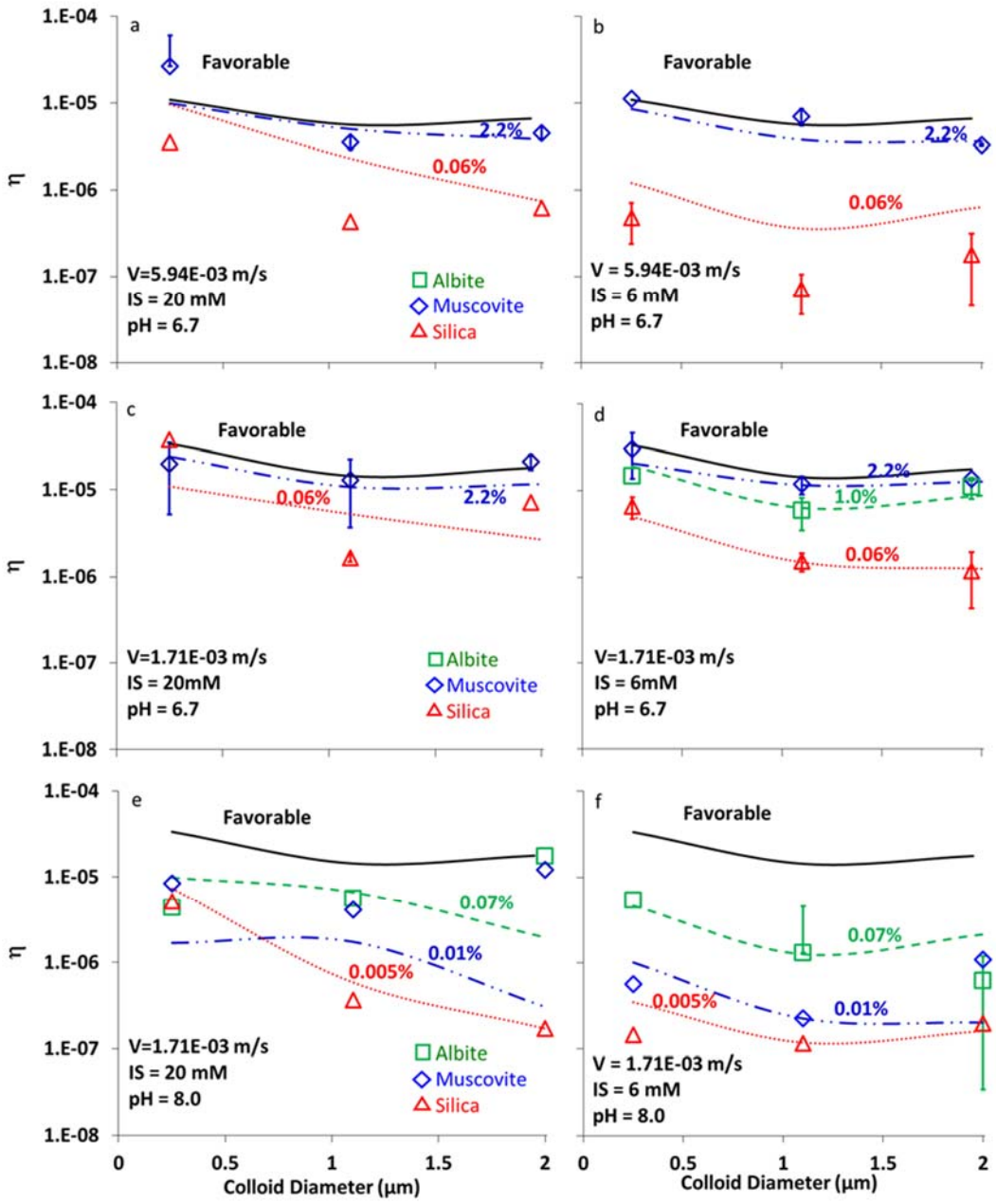

Figure 3 Experimentally observed collector efficiencies (η) as a function of colloid size for soda-lime glass (red triangles), muscovite (blue diamonds) and albite (green squares) at multiple ionic strengths (6mM, 20mM), pH values (6.7 and 8.0) and fluid velocities (1.71E-03, 5.94E-03 m/s). Lines are mechanistic force/torque balance simulations with conversion to η. Black solid lines represent favorable condition simulations (mass transfer independent of mineral surface). Colored textured lines represent unfavorable condition simulations (blue dash-dot=muscovite, red dot=glass, green dash=albite). A Pareto size distribution of heterodomains was approximated using a 1:4 ratio of 120 nm to 60 nm (radius) heterodomains, respectively. Surface coverage by heterodomains is reported adjacent to the simulation line.

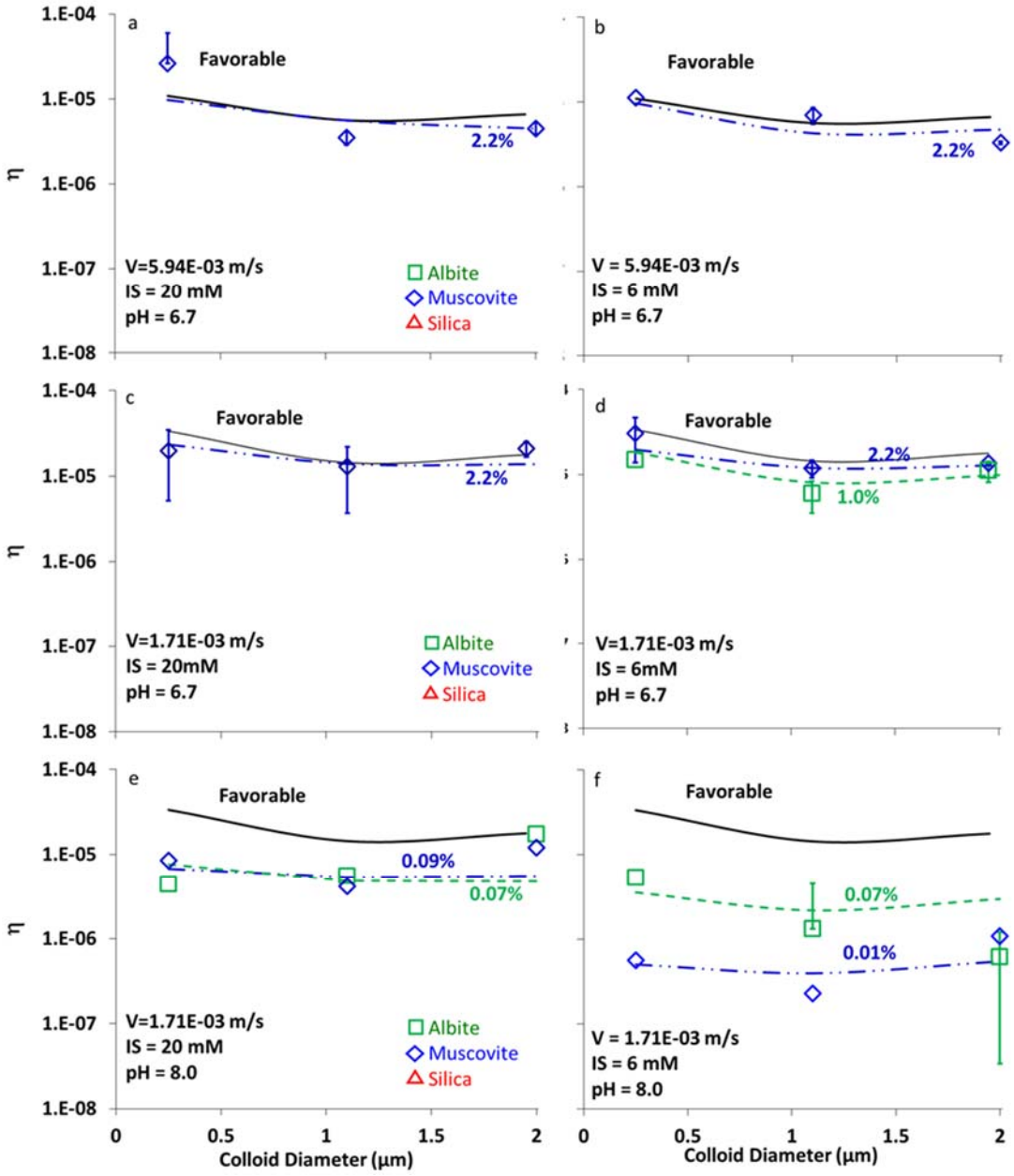

Figure 4 Experimentally-observed collector efficiencies (η) as a function of colloid size for soda-lime glass (red triangles), muscovite (blue diamonds) and albite (green squares) at multiple ionic strengths (6mM, 20mM), pH values (6.7 and 8.0) and fluid velocities (1.71E-03, 5.94E-03 m/s). Lines are mechanistic force/torque balance simulations with conversion to η. Black solid lines represent favorable condition simulations (mass transfer independent of mineral surface). Colored textured lines represent unfavorable condition simulations (blue dash-dot=muscovite, red dot=glass, green dash=albite). A uniform size distribution of 120nm (radius) heterodomains were used with heterodomain surface coverage (as function of total collector area) reported adjacent to simulation line.

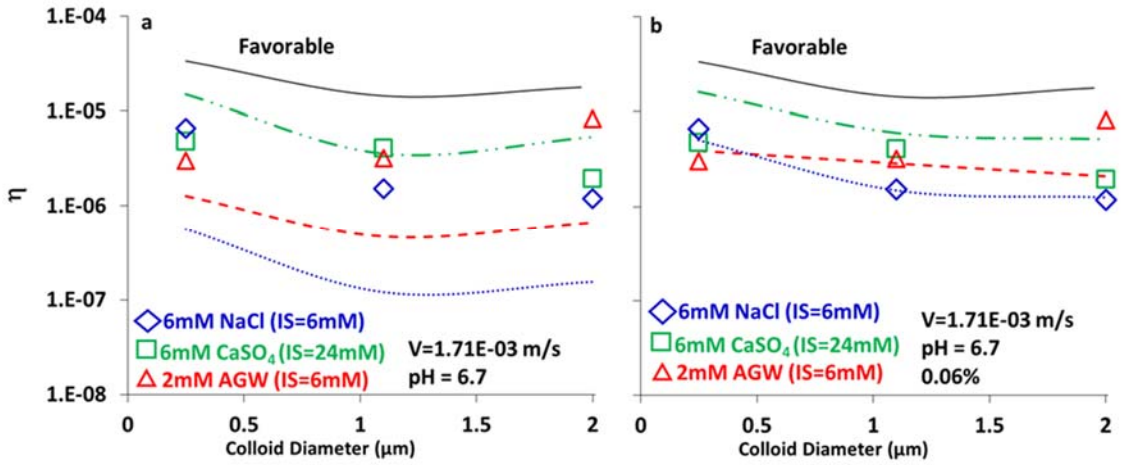

Figure 5 Experimentally observed collector efficiencies (η) as a function of colloid size for soda-lime glass in NaCl (blue diamonds), $CaSO_4$ (green squares) and artificial groundwater (AGW) (red triangles). Lines are mechanistic force/torque balance simulations with conversion to η. Black solid lines represent favorable condition simulations (mass transfer independent of mineral surface). Colored textured lines represent unfavorable condition simulations (blue dot=NaCl, red dash=AGW, green dash-dot=$CaSO_4$). Panel 'a' simulations were performed using a Pareto size distribution of heterodomains approximated using a 1:4 ratio of 120 nm to 60 nm (radius) heterodomains, respectively, using a surface coverage of 0.06%. Panel 'b' simulations were performed using Elimelech (1992) to obtain α, which was multiplied by simulated by η_{fav} values.

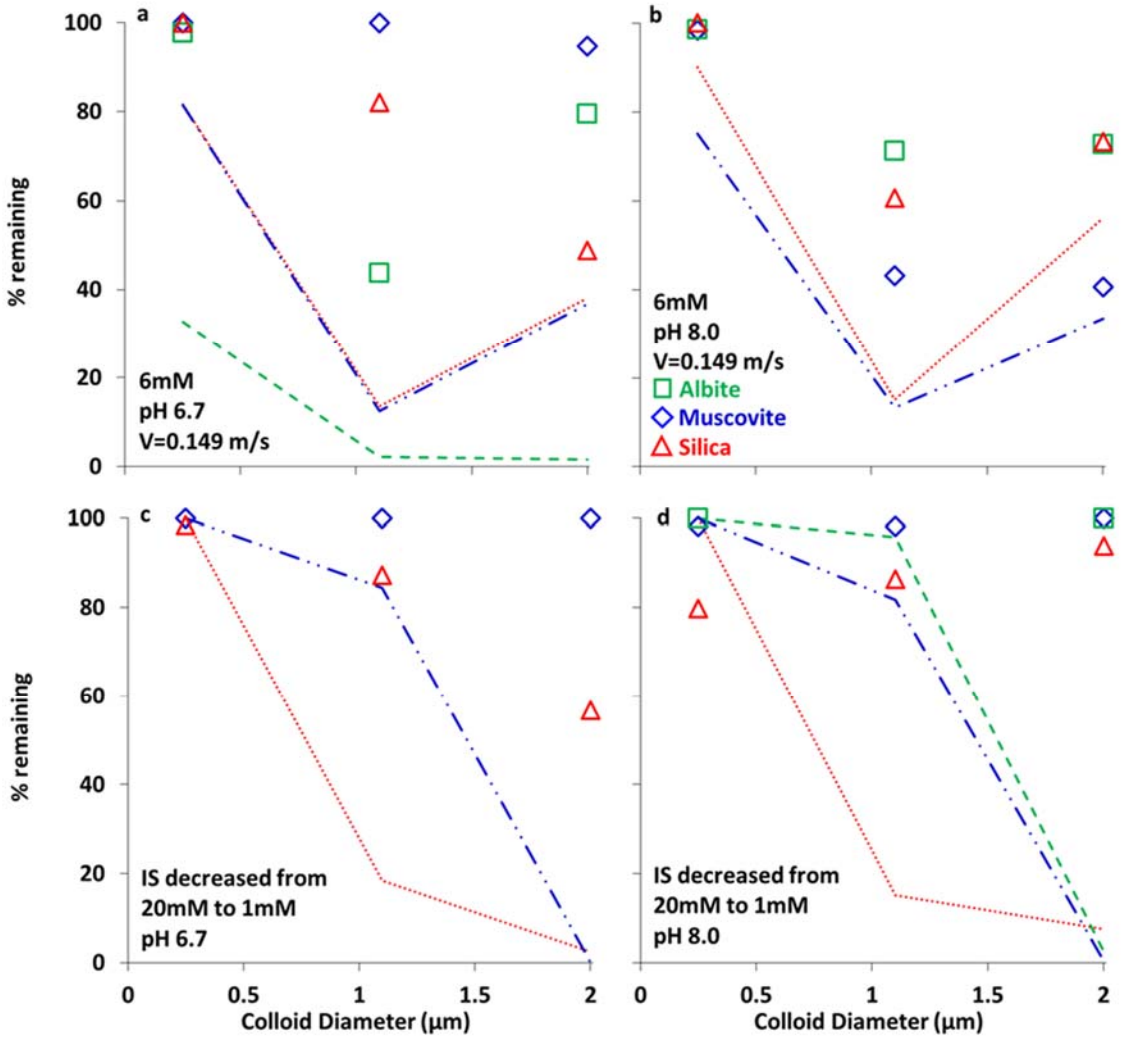

Figure 6 Experimentally-observed re-entrainment in response to 25x increased velocity following deposition under the 5.94×10^{-3} m/s velocity condition (a and b) and decrease in ionic strength (20 mM to 1 mM) (c and d) shown as a function of colloid size for soda-lime glass (red triangles), muscovite (blue diamonds), and albite (green squares) under two pH conditions (panel a = pH 6.7, panel b = pH 8.0). Colored textured lines are mechanistic simulations using modeling results from attachment simulations (red dots = glass, blue dash-dots = muscovite, green dashes = albite). Note: no experiments were run for 20mM pH 6.7 on albite and no release was seen in response to ionic strength perturbation at pH 8.0.

CHAPTER 5

DISCUSSION

The experimental results demonstrate that η_{unf} was influenced by mineral type (Figure 2). Muscovite and albite were shown to produce values of η_{unf} that approached η_{fav} under pH 6.7 conditions (Figure 2 a-d), whereas η_{unf} for muscovite was highly sensitive to pH under the IS = 6 mM condition (Figure1 e-f), possibly reflecting its higher IEP relative to silica and albite. As described above, sensitivity of η_{unf} among different mineral surfaces was not reasonably captured by semi-empirical expressions; however, the experimental trends in η_{unf} as a function of CML size (*ca*. 1-μm minimum) were reasonably reflected by the semi-empirical expressions. Simulations using representative discrete heterogeneity provided mineral-specific and pH-specific sensitivities of η_{unf} by varying heterodomain surface coverage among different minerals and among the different pH values (for a given mineral) (Figure 3). However, representation of the trends in η_{unf} as a function of CML size was achieved by additionally distinguishing the heterodomain size distribution among different mineral surfaces, i.e., Pareto-distributed heterodomains for silica and uniform heterodomain size for muscovite. Increasing heterodomain surface coverage for a given condition and mineral type will result in favorable conditions being achieved, but collector specific parameters (Hamaker Constant, ζ-potential) and heterodomain distribution result

in divergent trends between minerals in η as a function of heterodomain surface coverage (Figure 7).

The utility is apparent of specifying different discrete heterogeneity representations for different minerals and different pH values (for a given mineral). However, the resulting trends in η with CML size predicted by the discrete heterogeneity approach are sometimes more complicated relative to the experimentally observed trends. The experimentally observed minimum of η ca. 1.1 μm holds regardless of mineral type and pH, and it is reasonable to conclude that this predominant trend reflects an underlying parsimony that needs to be reflected in the models. The minimum of η ca. 1.1 μm reflects the relatively lesser diffusion, and sedimentation, of the *ca.* 1 μm colloid size relative to smaller and larger colloids, respectively. It is therefore reasonable to posit that the same processes shape the nearly equivalent trend repeatedly observed under unfavorable conditions. It is possible that the overcomplicated simulated trends result from ascribing all heterogeneity to the collector surface. Ascribing some form of heterogeneity to the colloid surface may allow greater influence of the colloid size on attachment, thereby potentially influencing the trend in η_{unf} as a function of colloid size in a way that is consistent with that observed under favorable conditions (tradeoff between diffusion and sedimentation). Since our results clearly demonstrate that η_{unf} is also influenced by mineral-specific characteristics, heterogeneity cannot be ascribed solely to the colloid. Adjusting the simulations to account for colloid heterogeneity may not be straightforward; i.e., it may require accounting for the rate of colloid rotation in the near-surface fluid, and so is a subject for future study. Another subject for future study is the direct and independent identification of specific heterogeneity attribute(s) (e.g., roughness and nanoscale chemical heterogeneity) of colloid

and collector surfaces through spectroscopic, atomic force, and other techniques.

Whereas we would not expect to quantitatively match experimental detachment results because of the dynamic nature of detachment and the representative nature of discrete heterogeneity, the comparisons demonstrate that the complex process of detachment is difficult to simulate. For example, as the torque balance involving contact mechanics is imposed in the closest few nm of separation distance, the simulations neglect diffusion for computational economy (Pazmino et al., 2014b). Quantitative prediction of detachment may be improved by inclusion of time-dependent processes that may increase colloid-collector attraction upon attachment. Particle-adhesion literature suggests the force required to detach a particle from a surface increases from the time of attachment, most significantly in the first 24 hours. This behavior has been attributed to a particle rotating into a more stable position (Butt et al., 1995). Increasing colloid-collector attraction through colloid settling onto a nanoscale asperity or a place of nanoscale heterogenity on the colloid may explain the differences in observed detachment compared to simulated attachment.

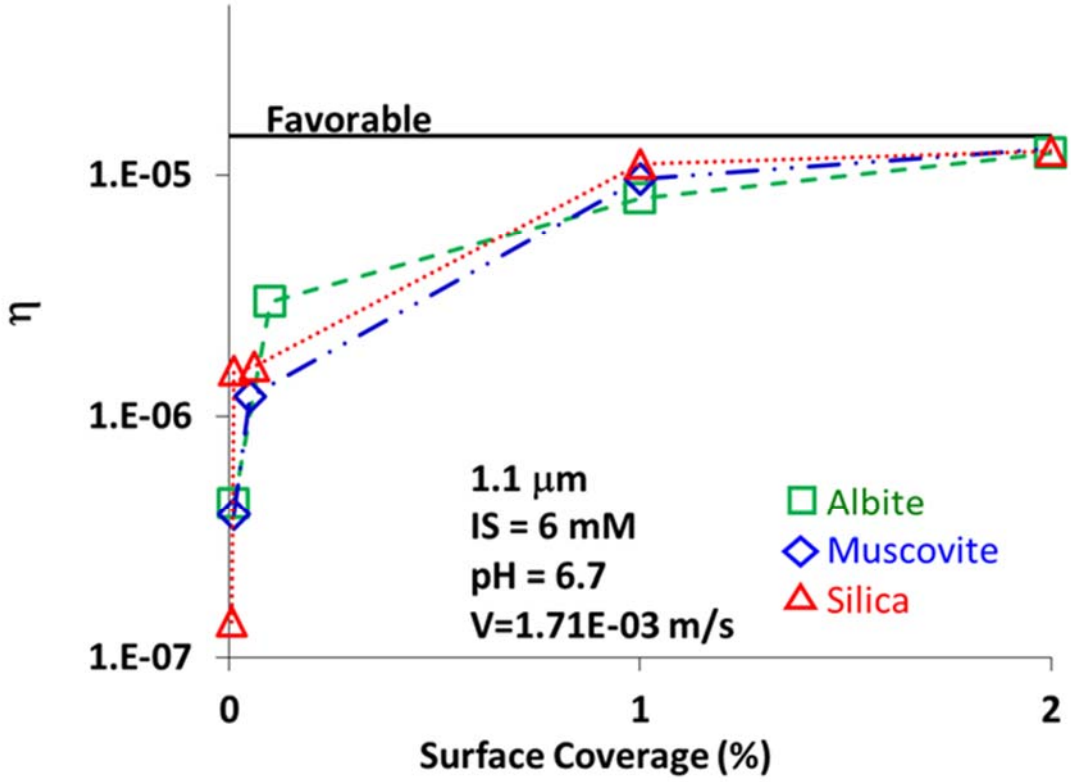

Figure 7 Simulated collector efficiency (η) as a function of surface coverage for a single colloid size and condition (1.1 μm, IS=6 mM NaCl, pH 6.7, 1.71×10^{-3} m/s) for different minerals.

CHAPTER 6

FUTURE WORK

We met our dual goals of examining colloid filtration in environmentally relevant conditions and testing the ability of the discrete heterogeneity approach to predict filtration under these conditions, but the work also revealed opportunities to further improve our understanding of filtration. The surfaces and conditions examined in this study are a good start to creating a more complete 'library' of surfaces that can allow for better prediction of colloid filtration in natural media. In addition to creating a library of different surfaces, there are some areas in which the discrete heterogeneity model can be improved. One shortcoming identified through this study was the model's failure to capture the behavior of the larger colloids across a range of different surfaces and solution chemistries. Inclusion of surface roughness as a form of heterogeneity may help improve predictions across different surfaces. Another area the model could be improved is the ability to predict the effect of solution pH on colloid filtration. In order to match the experimentally observed reduction in colloid retention at the high pH condition, the heterodomain surface coverage was reduced. While this approach worked, the model could include the isoelectric point of the surfaces as a parameter to allow the heterodomain surface coverage to vary with pH.

One of the significant improvements the discrete heterogeneity model offers over

previous approaches is its ability to simulate both attachment and detachment of colloids from surfaces. While the model is able to capture the trends of colloid detachment across a range of colloid sizes, it generally overpredicts detachment when compared to experimental observations. One approach to improving prediction of colloid detachment is inclusion of time-dependent attachment forces. The residence time versus colloid retention data matches previously published data, which suggests that deposited colloids may become more strongly attached over time. Making colloid-surface attraction after deposition a function of time in the model may improve prediction of colloid detachment.

Beyond improving the discrete heterogeneity model, the information gained from this investigation can be used to improve prediction using previously published equations. Work by Johnson and Elimelech has shown that filtration in macroscopically heterogeneous media can be successfully modeled using a piece-wise linear combination of favorable and unfavorable surfaces (Johnson and Elimelech, 1996). However, this approach failed in media dominated by unfavorable surfaces as it assumed a single, experimentally determined unfavorable collector efficiency for all conditions, regardless of solution chemistry (Johnson and Elimelech, 1996). The 'library of surfaces' and the ability of the discrete heterogeneity model to predict the effect of solution chemistry and fluid velocity under unfavorable conditions can improve prediction in macroscopically heterogeneous media that is dominated by unfavorable surfaces. The usefulness of this 'library' of surfaces in improving predictions in macroscopically heterogeneous media could be relatively easily tested by completing column-scale experiments of mixed media using the surfaces and solution chemistry conditions examined in this work and employing the approach pioneered by Johnson and Elimelech.

APPENDIX

SUPPORTING INFORMATION

Table 1 Artificial groundwater composition. Data source Ferris 2004.

Electrolyte	Concentration (mM)
K2SO4	0.00403
MgSO4	0.448
CaCl2	1.75
NaNO3	0.0044
NaHCO3	1.10
KHCO3	0.0623

Table 2 Zeta potential values used in simulations where CML=carboxylate modified polystyrene latex and DLS refers to calculations based on measurement on a dynamic light scattering instrument.

Material	Particle Size (um)	Electrolyte	Concentration (mM)	pH	zeta potential (mV)	Source
CML	0.25	NaCl	6	6.7	-35.7	DLS
CML	1.1	NaCl	6	6.7	-78.5	DLS
CML	2	NaCl	6	6.7	-79.2	DLS
CML	0.25	NaCl	20	6.7	-26	DLS
CML	1.1	NaCl	20	6.7	-48.9	DLS
CML	2	NaCl	20	6.7	-61.5	DLS
CML	0.25	NaCl	6	8	-40.8	DLS
CML	1.1	NaCl	6	8	-91	DLS
CML	2	NaCl	6	8	-80.5	DLS
CML	0.25	NaCl	20	8	-26.5	DLS
CML	1.1	NaCl	20	8	-62.2	DLS
CML	2	NaCl	20	8	-66.5	DLS
CML	0.25	CaSO4	1.5	6.7	-34.9	DLS
CML	1.1	CaSO4	1.5	6.7	-48.3	DLS
CML	2	CaSO4	1.5	6.7	-43.7	DLS
CML	0.25	CaSO4	6	6.7	-16.5	DLS
CML	1.1	CaSO4	6	6.7	-32.9	DLS
CML	2	CaSO4	6	6.7	-29.3	DLS
CML	0.25	AGW	1.8	6.7	-32.3	DLS
CML	1.1	AGW	1.8	6.7	-44.9	DLS
CML	2	AGW	1.8	6.7	-41.7	DLS
Soda-lime Glass	N/A	NaCl	6	6.7	-70	Kirby et al., 2004

Table 2 Continued

Material	Particle Size (um)	Electrolyte	Concentration (mM)	pH	zeta potential (mV)	Source
Soda-lime Glass	N/A	NaCl	20	6.7	-53.5	Kirby et al., 2004
Soda-lime Glass	N/A	NaCl	6	8	-80	Kirby et al., 2004
Soda-lime Glass	N/A	NaCl	20	8	-70	Kirby et al., 2004
Soda-lime Glass	N/A	CaSO4	1.5	6.7	-26.7	DLS
Soda-lime Glass	N/A	CaSO4	6	6.7	-19.2	DLS
Soda-lime Glass	N/A	AGW	1.8	6.7	-26.9	DLS
Muscovite	N/A	NaCl	6	6.7/8.0	-80	Scales et al., 1990
Muscovite	N/A	NaCl	20	6.7/8.0	-70	Scales et al., 1990
Albite	N/A	NaCl	6	6.7	-39	DLS
Albite	N/A	NaCl	6	8	-35.9	DLS
Albite	N/A	NaCl	20	8	-40.3	DLS

Table 3 Experimental re-entrainment data for glass in response to velocity increase (5x or 25x) or ionic strength (IS) reduction (20mM to 1mM).

Perturbation	Colloid Size (µm)	Velocity (mm/s)	IS (mM)	pH	% Re-entrained	% Remaining
IS	0.25	1.71	20	6.7	1.60	98.40
IS	1.1	1.71	20	6.7	12.80	87.20
IS	2	1.71	20	6.7	43.30	56.70
5x	0.25	5.94	6	6.7	0.00	100.00
5x	1.1	5.94	6	6.7	1.50	98.50
5x	2	5.94	6	6.7	1.65	98.35
25x	0.25	5.94	6	6.7	0.00	100.00
25x	1.1	5.94	6	6.7	17.90	82.10
25x	2	5.94	6	6.7	51.15	48.85
5x	0.25	1.71	6	8	11.11	88.89
5x	1.1	1.71	6	8	2.94	97.06
5x	2	1.71	6	8	8.70	91.30
25x	0.25	1.71	6	8	3.57	96.43
25x	1.1	1.71	6	8	15.15	84.85
25x	2	1.71	6	8	21.05	78.95
25xHV	0.25	1.71	6	8	0.00	100.00
25xHV	1.1	1.71	6	8	39.29	60.71
25xHV	2	1.71	6	8	26.67	73.33

Table 4 Experimental detachment data for CML on muscovite in response to velocity increase (5x or 25x) or ionic strength (IS) reduction (20mM-1mM).

Perturbation	Colloid Size (μm)	Velocity (mm/s)	IS (mM)	pH	% Re-entrained	% Remaining
5x, 25x	0.25	5.94	6	6.7	0.00	100.00
5x, 25x	1.1	5.94	6	6.7	0.00	100.00
5x	2	5.94	6	6.7	0.40	99.60
25x	2	5.94	6	6.7	5.30	94.70
5x	0.25	1.71	6	6.7	0.40	99.60
25x	0.25	1.71	6	6.7	0.20	99.80
5x, 25x	1.1	1.71	6	6.7	0.00	100.00
5x, 25x	2	1.71	6	6.7	0.00	100.00
5x, 25x, IS	0.25	5.94	20	6.7	0.00	100.00
5x, IS	1.1	5.94	20	6.7	0.00	100.00
25x	1.1	5.94	20	6.7	22.10	77.90
5x, IS	2	5.94	20	6.7	0.00	100.00
25x	2	5.94	20	6.7	17.30	82.70
5x, 25x, IS	0.25	1.71	20	6.7	0.00	100.00
5x, 25x	1.1	1.71	20	6.7	0.00	100.00
5x, 25x	2	1.71	20	6.7	0.00	100.00
5x	0.25	1.71	6	8	2.20	97.80
25x	0.25	1.71	6	8	0.00	100.00
5x	1.1	1.71	6	8	17.30	82.70
25x	1.1	1.71	6	8	15.90	84.10
5x	2	1.71	6	8	8.90	91.10
25x	2	1.71	6	8	24.00	76.00
5x, 25x	1.1	1.71	20	8	0.00	100.00
5x, 25x	2	1.71	20	8	0.00	100.00
25xHV	0.25	1.71	6	8	1.61	98.39
25xHV	1.1	1.71	6	8	56.80	43.20
25xHV	2	1.71	6	8	59.30	40.70

Table 5 Experimental detachment data for CML on albite in response to velocity increase (5x or 25x) or ionic strength (IS) reduction (20mM-1mM).

Perturbation	Colloid Size (μm)	Velocity (mm/s)	IS (mM)	pH	% Re-entrained	% Remaining
5x, 25x	0.25	1.71	6	6.7	0	100
25xHV	0.25	1.71	6	6.7	2.2	97.8
5x	1.1	1.71	6	6.7	2.15	97.85
25x	1.1	1.71	6	6.7	6.55	93.45
25xHV	1.1	1.71	6	6.7	56.3	43.7
5x, 25x	2	1.71	6	6.7	0	100
25xHV	2	1.71	6	6.7	20.5	79.5
5x	0.25	1.71	6	8	1.5	98.5
25x	0.25	1.71	6	8	0	100
25xHV	0.25	1.71	6	8	1.5	98.5
5x	1.1	1.71	6	8	4.8	95.2
25x	1.1	1.71	6	8	19.3	80.7
25xHV	1.1	1.71	6	8	44.1	55.9
5x	2	1.71	6	8	0	100
25x	2	1.71	6	8	12.1	87.9
25xHV	2	1.71	6	8	27.35	72.65
IS	0.25	1.71	20	8	0	100
5x,IS	1.1	1.71	20	8	0	100
25x	1.1	1.71	20	8	1.25	98.75
IS	2	1.71	20	8	0	100

Table 6 Experimental residence times for colloids in response to velocity perturbation

Perturbation Type	Collector Material	Colloid Size (μm)	Velocity (mm/s)	IS (mM)	pH	Residence Time Remaining Colloids (s)	Residence Time Detached Colloids (s)
Velocity	Silica	1.1	149	6	8.0	13765	7539
Velocity	Silica	2.0	149	6	8.0	19448	18263
Velocity	Muscovite	1.1	149	6	8.0	3774	909
Velocity	Muscovite	2.0	149	6	8.0	4756	3055
Velocity	Albite	1.1	149	6	8.0	2952	3462
Velocity	Albite	2.0	149	6	8.0	5536	5728

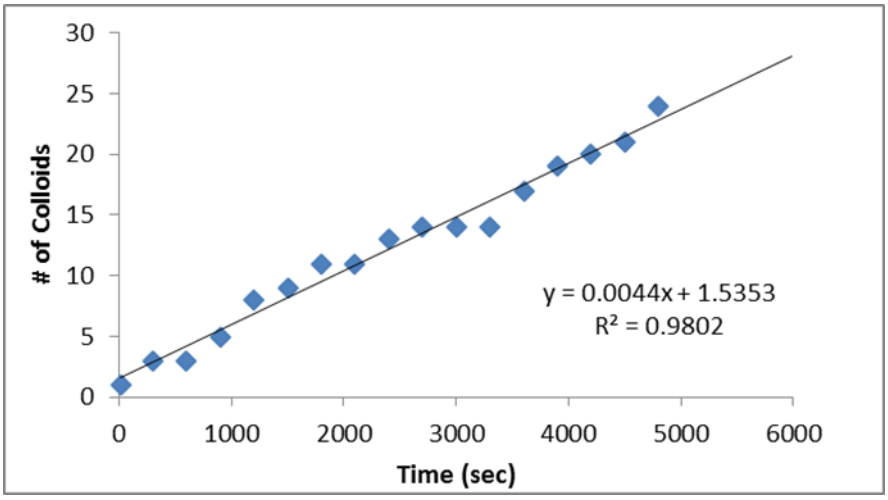

Figure 8 Number of colloids on surface as a function of time, experimental data from an impinging jet experiment on muscovite, 5.94×10^{-3} m/s, 6 mM, pH 6.7.

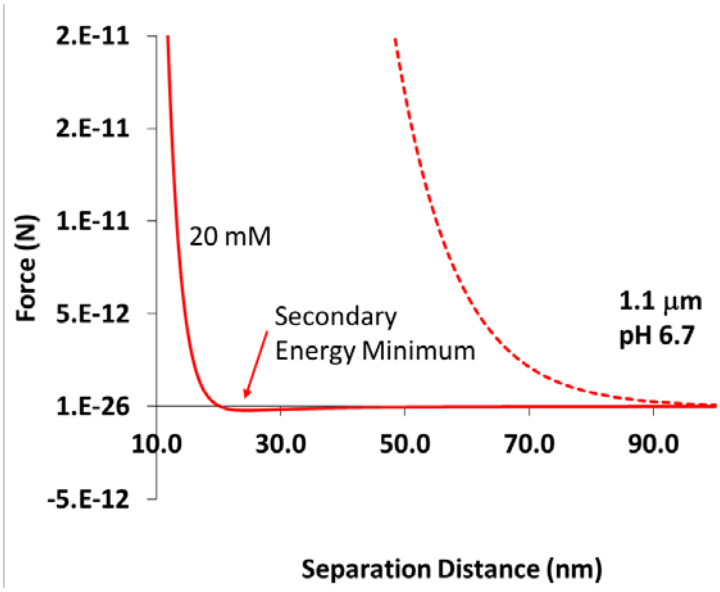

Figure 9 Calculated colloidal forces (DLVO + steric) as a function of separation distance for a 1.1 μm colloid in 20 mM (solid) and 1 mM (dashed) at pH 6.7 showing the presence and lack of a secondary energy minimum.

REFERENCES

Abbott, A., Rutter, P.R. and Berkeley, R.C., 1983. The Influence of Ionic Strength, Ph and a Protein Layer on the Interaction Between Streptococcus Mutans and Glass Surfaces. *J Gen Microbio*l, 129(2): 439-45.

Ackler, H.D., French, R.H. and Chiang, Y.-M., 1996. Comparisons of Hamaker Constants for Ceramic Systems with Intervening Vacuum or Water: From Force Laws and Physical Properties. *Journal of Colloid and Interface Science,* 179(2): 460-469.

Adamczyk, Z., Zaucha, M. and Zembala, M., 2010. Zeta Potential of Mica Covered by Colloid Particles: A Streaming Potential Study. *Langmuir*, 26(12): 9368-9377.

Bai, R.B. and Tien, C., 1999. Particle Deposition under Unfavorable Surface Interactions. *Journal of Colloid and Interface Science*, 218(2): 488-499.

Bendersky, M. and Davis, J.M., 2011. DLVO Interaction of Colloidal Particles with Topographically and Chemically Heterogeneous Surfaces. *Journal of Colloid and Interface Science*, 353(1): 87-97.

Bergström, L., 1997. Hamaker Constants of Inorganic Materials. *Advances in Colloid and Interface Science*, 70(0): 125-169.

Butt, H.-J.; Jaschke, M.; Ducker, W., Measuring Surface Forces in Aqueous Electrolyte Solution with the Atomic Force Microscope. *Bioelectrochemistry and Bioenergetics* **1995,** *38* (1), 191-201.

Chang, Y.I., Cheng, W.Y. and Chan, H.C., 2009. A Proposed Correlation Equation for Predicting Filter Coefficient under Unfavorable Deposition Conditions. *Separation and Purification Technology*, 65(3): 248-250.

Chen, G. and Walker, S.L., 2007. Role of Solution Chemistry and Ion Valence on the Adhesion Kinetics of Groundwater and Marine Bacteria. *Langmuir,* 23(13): 7162-7169.

Deer, W.A., Howie, R.A. and Zussman, J., 2001. Rock-forming Minerals: Feldspars, Volume 4A. Geological Society.

Duffadar, R., Kalasin, S., Davis, J.M. and Santore, M.M., 2009. The Impact of Nanoscale Chemical Features on Micron-Scale Adhesion: Crossover from Heterogeneity-Dominated to Mean-Field Behavior. *Journal of Colloid and Interface Science*, 337(2): 396-407.

Duffadar, R.D. and Davis, J.M., 2007. Interaction of Micrometer-Scale Particles with Nanotextured Surfaces in Shear Flow. *Journal of Colloid and Interface Science*, 308(1): 20-29.

Duffadar, R.D. and Davis, J.M., 2008. Dynamic Adhesion Behavior of Micrometer-Scale Particles Flowing over Patchy Surfaces with Nanoscale Electrostatic Heterogeneity. *Journal of Colloid and Interface Science*, 326(1): 18-27.

Elimelech, M., 1992. Predicting Collision Efficiencies of Colloidal Particles in Porous Media. *Water Research*, 26(1): 1-8.

Elimelech, M., Nagai, M., Ko, C.-H. and Ryan, J.N., 2000a. Relative Insignificance of Mineral Grain Zeta Potential to Colloid Transport in Geochemically Heterogeneous Porous Media. *Environmental Science & Technology*, 34(11): 2143-2148.

Elimelech, M., Nagai, M., Ko, C.-H. and Ryan, J.N., 2000b. Relative Insignificance of Mineral Grain Zeta Potential to Colloid Transport in Geochemically Heterogeneous Porous Media. *Environmental Science and Technology*, 34(11): 2143-2148.

Elimelech, M. and O'Melia, C.R., 1990. Kinetics of Deposition of Colloidal Particles in Porous Media. *Environmental Science and Technology*, 1528-1536.

Ferris, F., Phoenix, V., Fujita, Y. and Smith, R., 2004. Kinetics of Calcite Precipitation Induced by Ureolytic Bacteria at 10 To 20 C in Artificial Groundwater. *Geochimica et Cosmochimica Acta*, 68(8): 1701-1710.

Gregory, J., 1981. Approximate Expressions for Retarded Van Der Waals Interaction. *Journal of Colloid and Interface Science*, 83(1): 138-45.

Hoek, E.M.V., Bhattacharjee, S. and Elimelech, M., 2003. Effect of Membrane Surface Roughness on Colloid−Membrane DLVO Interactions. *Langmuir,* 19(11): 4836-4847.

Israelachvili, J., 2011. Intermolecular and Surface Forces 3rd Edition. *Elseveier*.

Jewett, D.G., Hilbert, T.A., Logan, B.E., Arnold, R.G. and Bales, R.C., 1995. Bacterial Transport in Laboratory Columns and Filters: Influence of Ionic Strength and Ph on Collision Efficiency. *Water Research,* 29(7): 1673-1680.

Johnson, P.R., Sun, N. and Elimelech, M., 1996. Colloid Transport in Geochemically Heterogeneous Porous Media: Modeling and Measurements. *Environmental Science & Technology*, 30(11): 3284-3293.

Johnson, W.P. and Tong, M., 2006. Observed and Simulated Fluid Drag Effects on Colloid Deposition in the Presence of an Energy Barrier in an Impinging Jet System. *Environmental Science and Technology,* 40(16): 5015-5021.

Kern, W., 1970. Cleaning Solutions Based on Hydrogen Peroxide for Use in Silicon Semiconductor Technology. *RCA Review*, 31: 187-206.

Kirby, B.J. and Hasselbrink, E.F., 2004. Zeta Potential of Microfluidic Substrates: 1. Theory, Experimental Techniques, and Effects on Separations. *Electrophoresis,* 25(2): 187-202.

Kosmulski, M., 2011. The pH-Dependent Surface Charging and Points of Zero Charge: V. Update. *Journal of Colloid and Interface Science*, 353(1): 1-15.

Laumann, S., Micić, V. and Hofmann, T., 2014. Mobility Enhancement of Nanoscale Zero-Valent Iron in Carbonate Porous Media Through Co-Injection of Polyelectrolytes. *Water Research*, 50(0): 70-79.

Lin, S. and Wiesner, M.R., 2012. Theoretical Investigation on the Interaction Between a Soft Particle and a Rigid Surface. *Chemical Engineering Journal*, 191(0): 297-305.

Liu, D., Johnson, P.R. and Elimelech, M., 1995. Colloid Deposition Dynamics in Flow-Through Porous Media: Role of Electrolyte Concentration. *Environmental Science & Technology*, 29(12): 2963-2973.

Liu, J., Miller, J.D., Yin, X., Gupta, V. and Wang, X., 2014. Influence of Ionic Strength on the Surface Charge and Interaction of Layered Silicate Particles. *Journal of Colloid and Interface Science*, 432(0): 270-277.

Loveland, J.P., Bhattacharjee, S., Ryan, J.N. and Elimelech, M., 2003. Colloid Transport in a Geochemically Heterogeneous Porous Medium: Aquifer Tank Experiment and Modeling. *Journal of Contaminant Hydrology,* 65(3–4): 161-182.

Ma, H., Pazmino, E. and Johnson, W.P., 2011. Surface Heterogeneity on Hemispheres-In-Cell Model Yields all Experimentally-Observed Non-Straining Colloid Retention Mechanisms in Porous Media in the Presence of Energy Barriers. *Langmuir,* 27(24): 14982-14994.

Maier, R.M. and Pepper, I.L., 2009. Chapter 4 - Earth Environments. In: R.M.M.L.P.P. Gerba (Editor), *Environmental Microbiology (Second Edition)*. Academic Press, San Diego, pp. 57-82.

Ohshima, H., 1995. Electrophoretic Mobility of Soft Particles. Colloids and Surfaces A: Physicochemical and Engineering Aspects, 103(3): 249-255.

Olhoeft, G.R., 1989. Electrical Properties of Rocks. Physical Properties of Rocks and Minerals, Section 2. CRC Press, Boca Raton, FL.

Pazmino, E., Trauscht, J., Dame, B. and Johnson, W.P., 2014a. Power Law Size-Distributed Heterogeneity Explains Colloid Retention on Soda Lime Glass in the Presence of Energy Barriers. *Langmuir,* 30(19): 5412-5421.

Pazmino, E., Trauscht, J. and Johnson, W.P., 2014b. Release of Colloids from Primary Minimum Contact under Unfavorable Conditions by Perturbations in Ionic Strength and Flow Rate. *Environmental Science & Technology*, 48(16): 9227-9235.

Rajagopalan, R. and Tien, C., 1976. Trajectory Analysis of Deep-Bed Filtration with the Sphere-In-Cell Porous Media Model. *Aiche Journal,* 22(3): 523-533.

Rosenholtz, J.L.R.S., Dudley T., 1936. The Dielectric Constant of Mineral Powders. *Rensselaer Polytechnic Institute Engineering and Science Series 52*.

Scales, P.J., Grieser, F. and Healy, T.W., 1990. Electrokinetics of the Muscovite Mica-Aqueous Solution Interface. *Langmuir*, 6(3): 582-589.

Song, L., Johnson, P.R. and Elimelech, M., 1994. Kinetics of Colloid Deposition onto Heterogeneously Charged Surfaces in Porous Media. *Environmental Science and Technology*, 28(6): 1164-1164.

Tufenkji, N. and Elimelech, M., 2004. Correlation Equation for Predicting Single-Collector Efficiency in Physicochemical Filtration in Saturated Porous Media. *Environmental Science and Technology*, 38(2): 529-536.

Weiss, W.J., Bouwer, E.J., Aboytes, R., LeChevallier, M.W., O'Melie, C.R., Le, B.T. and Schwab, K.J., 2005. Riverbank Filtration for Control Of Microorganisms: Results From Field Monitoring. *Water Research*, 59: 1990-2001.

Yao, K.-M., Habibian, M.T. and O'Melia, C.R., 1971. Water and Waste Water Filtration: Concepts and Applications. *Environmental Science and Technology*, 5(11): 1105-1112.

Zhang, W.-x., 2003. Nanoscale Iron Particles for Environmental Remediation: An Overview. *Journal of Nanoparticle Research,* 5(3-4): 323-332.